HHS Public Access

Author manuscript

Cell Rep. Author manuscript; available in PMC 2017 September 26.

Published in final edited form as:

Cell Rep. 2017 August 08; 20(6): 1409–1421. doi:10.1016/j.celrep.2017.07.041.

Vesicle Docking Is a Key Target of Local PI(4,5)P_2 Metabolism in the Secretory Pathway of INS-1 Cells

Chen Ji[1], **Fan Fan**[1], and **Xuelin Lou**[1,2,*]

[1]Department of Neuroscience, School of Medicine and Public Health, University of Wisconsin-Madison, Madison, WI 53705, USA

SUMMARY

Phosphatidylinositol 4,5-bisphosphate (PI(4,5)P_2) signaling is transient and spatially confined in live cells. How this pattern of signaling regulates transmitter release and hormone secretion has not been addressed. We devised an optogenetic approach to control PI(4,5)P_2 levels in time and space in insulin-secreting cells. Combining this approach with total internal reflection fluorescence microscopy, we examined individual vesicle-trafficking steps. Unlike long-term PI(4,5)P_2 perturbations, rapid and cell-wide PI(4,5)P_2 reduction in the plasma membrane (PM) strongly inhibits secretion and intracellular Ca^{2+} concentration ($[Ca^{2+}]_i$) responses, but not sytaxin1a clustering. Interestingly, local PI(4,5)P_2 reduction selectively at vesicle docking sites causes remarkable vesicle undocking from the PM without affecting $[Ca^{2+}]_i$. These results highlight a key role of local PI(4,5)P_2 in vesicle tethering and docking, coordinated with its role in priming and fusion. Thus, different spatiotemporal PI(4,5)P_2 signaling regulates distinct steps of vesicle trafficking, and vesicle docking may be a key target of local PI(4,5)P_2 signaling in vivo.

Graphical Abstract

Spatiotemporal precision in cell signaling is key to its efficiency and specificity. By controlling PI(4,5)P_2 levels in space and time with optogenetic approaches, Ji et al. uncover a critical role of PI(4,5)P_2 at vesicle-release sites in stabilizing vesicle tethering and docking at the plasma membrane.

*Correspondence: xlou3@wisc.edu.

[2]Lead Contact

SUPPLEMENTAL INFORMATION

Supplemental Information includes Supplemental Experimental Procedures, five figures, and seven movies and can be found with this article online at http://dx.doi.org/10.1016/j.celrep.2017.07.041.

AUTHOR CONTRIBUTIONS

C.J., F.F., and X.L. designed research; C.J. performed experiments; C.J. and X.L. analyzed data; F.F. initiated the project and performed pilot experiments and data analysis; and C.J. and X.L. wrote the manuscript.

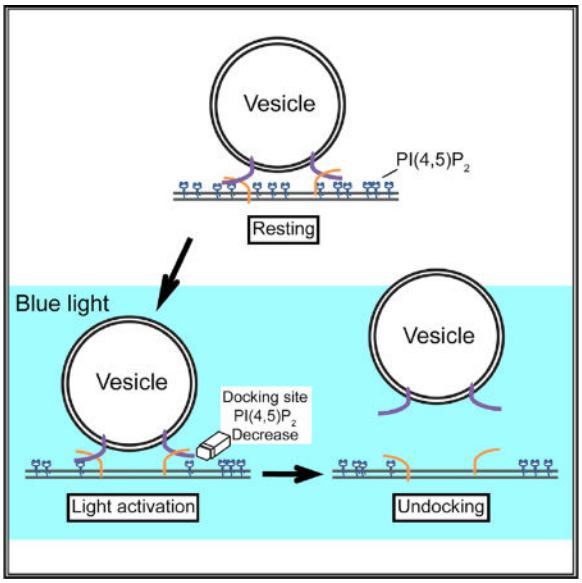

INTRODUCTION

Phosphatidylinositol-4,5-bisphosphate ($PI(4,5)P_2$) is relatively abundant among phosphoinositides (PIs) in theplasmamembrane (PM) (Ji et al., 2015; Hammond et al., 2012; Nakatsu et al., 2012). It regulates cellular function (De Camilli et al., 1996; Di Paolo and De Camilli, 2006; Balla, 2013) by interacting directly with its effector proteins and/or serving as a precursor of second messengers (Martin, 2015; Hammond and Balla, 2015; Di Paolo and De Camilli, 2006). Biochemical and genetic studies have demonstrated that $PI(4,5)P_2$ is required for both synaptic transmission (Wenk et al., 2001; Di Paolo et al., 2004; Cremona et al., 1999) and hormone secretion (Hay et al., 1995; Milosevic et al., 2005; Holz et al., 2000; Martin, 2001; James et al., 2008). Accordingly, in vitro experiments from liposome fusions (Bai et al., 2004) and membrane sheets (Honigmann et al., 2013) suggest a critical role of $PI(4,5)P_2$ for exocytosis. Spatially confined subcellular $PI(4,5)P_2$ signaling is widely thought to be crucial for signal specificity and efficiency in vivo. The presence of local $PI(4,5)P_2$ elevations at vesicle fusion sites (Trexler et al., 2016) indicates its specific role during exocytosis. However, all the available studies on $PI(4,5)P_2$-regulated exocytosis are based on either cell-wide $PI(4,5)P_2$ perturbation assays or in vitro experiments. The function of subcellular $PI(4,5)P_2$ signaling during exocytosis remains poorly understood.

During transmitter release and hormone secretion, secretory vesicles undergo different trafficking steps prior to exocytosis: vesicle recruitment from a distant reserve vesicle pool; tethering/docking to the PM; priming; and fusion upon Ca^{2+} triggering (Rettig and Neher, 2002; Voets, 2000; Neher and Sakaba, 2008; Imig et al., 2014; Südhof, 2013). Different roles of $PI(4,5)P_2$ have been reported in those processes. Biochemistry work has identified that a phosphatidylinositol transfer protein and a type I PIP5 kinase are required for vesicle secretion (Hay et al., 1995; Hay and Martin, 1993). Genetic knockout (KO) of major $PI(4,5)P_2$ metabolic enzymes synaptojanin-1 (Cremona et al., 1999) and PIP kinase type 1γ (PIPK1γ) (Di Paolo et al., 2004) severely impair clathrin-mediated endocytosis (CME),

vesicle uncoating (Cremona et al., 1999), and readily releasable pool (RRP) size (Di Paolo et al., 2004). Overexpression of membrane-targeted synaptojanin-1 and knockdown of PIPK1γ in chromaffin cells decrease RRP size and vesicle-refilling rate (Milosevic et al., 2005), implying a defect upstream of the Ca^{2+} triggering. PIPK1γ KO in chromaffin cells showed a selective defect in vesicle priming rather than vesicle docking and Ca^{2+} currents (Gong et al., 2005). On the other hand, $PI(4,5)P_2$ regulates Ca^{2+} channels (Suh et al., 2010); the supra-linear dependence between intracellular Ca^{2+} concentration (Lou et al., 2005) predicts a critical role of $PI(4,5)P_2$-mediated Ca^{2+} signaling in exocytosis. Moreover, all the previous studies employed either in vitro assays or cell-wide $PI(4,5)P_2$ perturbations, which lack subcellular specificity and often suffer from chronic interruptions that may induce adaptation. Thus, a long-standing question is how the fast, localized $PI(4,5)P_2$ alterations regulate exocytosis in the context of physiology.

The big challenge to address this question is the lack of approach for local $PI(4,5)P_2$ manipulations in living cells. Most previous studies rely on pharmacological or genetic perturbations of key enzymes for PI metabolism, in which cell-wide perturbations can evoke non-specific signaling and thus complicate data interpretations. Recent technology development makes it possible to overcome this issue. For example, chemical-inducible approaches, including rapamycin-induced FRB/FKBP12 dimers (Suh et al., 2006; Szentpetery et al., 2010; Heo et al., 2006; Varnai et al., 2006; Hammond et al., 2012), can rapidly control $PI(4,5)P_2$ signaling in live cells. The light-inducible heterodimerization method provides an optogenetic strategy to interrogating subcellular function in time and space (Toettcher et al., 2011; Pathak et al., 2013). Multiple light-switchable systems based on natural or engineered photoreceptors have been reported, such as light-inducible cryptochrome 2 (CRY2)/CIB1 dimers from *Arabidopsis thaliana* (Kennedy et al., 2010; Idevall-Hagren et al., 2012) and light-oxygen-voltage (LOV) domains (Yazawa et al., 2009). Light-inducible transportation of small organelles using motor protein (kinesin or dynein) has also been demonstrated recently in live cells (van Bergeijk et al., 2015; Duan et al., 2015).

Here, we developed an optogenetic approach for local $PI(4,5)P_2$ manipulations in time and space (e.g., specifically at vesicle docking sites) and dissected the role of $PI(4,5)P_2$ in vesicle trafficking in INS-1 cells. Total internal reflection fluorescence microscopy (TIRFM) allows monitoring temporal-spatial-dependent $PI(4,5)P_2$ regulation on each step of vesicle trafficking. We found different effects of $PI(4,5)P_2$ in vesicle trafficking, depending on its spatial and temporal patterns. In particular, rapid and local $PI(4,5)P_2$ signaling at vesicle-PM-contacting sites is crucial for stabilizing vesicle tethering and docking, a previously unappreciated effect upstream of vesicle priming in the secretory pathway. This function may be a key mechanism for $PI(4,5)P_2$-mediated exocytosis regulation in vivo, where fast and localized $PI(4,5)P_2$ metabolism occurs frequently.

RESULTS

Visualizing Vesicle Dynamics and Fusion under TIRFM after Chronic PI(4,5)P_2 Perturbations

We studied PI(4,5)P_2 function in insulin release in INS-1 cells using TIRFM (Axelrod, 1981; Zenisek et al., 2000). The 4-color TIRFM (Fan et al., 2015) allows us to visualize individual insulin granules in live cells and study their dynamics and exocytosis. We first evaluated the role of long-term PI(4,5)P_2 inhibition by overexpressing PI(4,5)P_2 binding domain of PLCδ1 ($PH_{PLC\delta1}$) (Hammond and Balla, 2015; Holz et al., 2000) for 2 days to compete with endogenous PI(4,5)P_2 effectors. Insulin granule exocytosis was imaged by NPY-pHluorin (Figure 1A; Movie S1), a pH-sensitive fluorescent probe for detecting large dense core vesicle (LDCV) fusion (Fan et al., 2015). During 60 mM KCl stimulation (for 7 min), exocytosis events tended to decrease (Figures 1B and 1C; $p > 0.05$) in the cells co-expressing mCherry-$PH_{PLC\delta1}$. The vesicle density under TIRFM labeled by NPY-DsRed, a granule marker colocalized with insulin granules (data not shown), was comparable to control (Figures 1D and 1E). Particle-tracking analysis revealed faster insulin granule dynamics than controls (Figure 1F), suggesting altered vesicle transportation due to the chronic PI(4,5)P_2 perturbations.

Syntaxin1a molecules form clusters on the PM (Ji et al., 2015; Bar-On et al., 2012; Barg et al., 2010; Sieber et al., 2007; Rickman et al., 2010), which may stabilize vesicle docking and promote priming (Barg et al., 2010; Gandasi and Barg, 2014) through their interactions with PI(4,5)P_2 (van den Bogaart et al., 2011; Aoyagi et al., 2005). Next, we examined synatxin1a alteration after overexpression of $PH_{PLC\delta1}$ in INS-1 cells. We found a significant decrease in EGFP-syntaxin1a cluster density (Figures 1G and 1H). This inhibitory effect correlated quantitatively with the levels of $PH_{PLC\delta1}$ expressed (Figure 1I), suggesting a decrease of free PI(4,5)P_2 accessible by endogenous effectors. The limited secretion inhibition may result from insufficient $PH_{PLC\delta1}$ expression levels or/and chronic PI(4,5)P_2 compensation in these cells. This result is consistent with the involvement of syntaxin1a cluster changes in modulating exocytosis following long-term PI(4,5)P_2 perturbations.

Distinct Effects of Rapid Optogenetic Control of PI(4,5)P_2 Metabolism on Vesicle Dynamics and Secretion from Chronic PI(4,5)P_2 Perturbations

To rapidly control PI(4,5)P_2 levels in living INS-1 cells, we developed an optogenetic approach (Figure 2A) by utilizing the improved light-inducible dimer (iLID) (Guntas et al., 2015) and an inositol polyphosphate-5-phosphatase domain of oculocerebrorenal syndrome of Lowe (OCRL) gene ($5'Ptase_{OCRL}$; Idevall-Hagren et al., 2012). We chose the iLID pair and $5'Ptase_{OCRL}$ because this combination can achieve the least background PI(4,5)P_2 perturbation in the dark (Hallett et al., 2016) and more efficient PI(4,5)P_2 depletion under blue light activation (Idevall-Hagren et al., 2012). $5'Ptase_{OCRL}$ was fused with the Micro (the cytosolic part of dimer), the other part of the dimer (iLID) was tagged with a CAAX sequence for the PM targeting, and both segments were further combined into a single iLID construct (tgRFPt-Micro-$5'Ptase_{OCRL}$-T2A-iLIDcaax) by inserting a T2A sequence in between (Figure 2A, bottom). This latter step is critical to boost transfection efficiency and maintain secretion capacity of INS-1 cells.

We expressed this plasmid and iRFP-$PH_{PLC\delta1}$ (an infra-red $PI(4,5)P_2$ probe) to control and image $PI(4,5)P_2$ levels simultaneously in INS-1 cells (Figure 2B). Blue light triggered rapid $5'Ptase_{OCRL}$ translocation to the PM and subsequent iRFP-$PH_{PLC\delta1}$ dissociation from the PM to cytosol (Figure 2B; Movie S2). The $PI(4,5)P_2$ levels (indicated by iRFP-$PH_{PLC\delta1}$) decreased immediately after light activation and reached a steady state within ~0.5 min (τ = 8.3 ± 1.1 s; n = 13 cells) as measured by TIRF imaging (Figure 2C). This response was reversible. It recovered within several minutes (τ = 70.5 ± 4.8 s; n = 13 cells) after stopping blue light illumination. Because $5'Ptase_{OCRL}$ converts $PI(4,5)P_2$ into PI4P after recruiting to the PM (without generating IP3), the iRFP-$PH_{PLC\delta1}$ dissociation from the PM suggested a specific decrease of $PI(4,5)P_2$ on the PM.

Using this optogenetic approach, we examined the effect of a rapid $PI(4,5)P_2$ decrease on vesicle trafficking in living INS-1 cells, in order to compare with the chronic perturbation of $PI(4,5)P_2$ (Figure 1). In the cells expressing iLIDs (tgRFPt-Micro-$5'Ptase_{OCRL}$-T2A-iLIDcaax) and NPY-pHluorin, blue light exposure led to a drastic decrease of fusion events induced by 60 mM KCl stimulation, in contrast with the control cells that expressed tgRFPt-Micro-$5'Ptase_{OCRL}$ (without the membrane anchor) and NPY-pHluorin (Figures 2D, 2F, and 2G). This is consistent with the result from bulk measurement of human growth hormone release in MIN6 cells (Xie et al., 2016). Interestingly, after $PI(4,5)P_2$ reduction, abundant NPY granules were still visible under the TIRF field with 405 excitation (Figure 2E), indicating a defect downstream of vesicle docking in the secretory pathway (e.g., vesicle priming, Ca^{2+} triggering, or fusion). Next, we monitored how the acute, global $PI(4,5)P_2$ decreases affect granule docking/tethering and dynamics. Quantitative analysis (Figures 2H and 2I) revealed a moderate decrease in granule density beneath the PM after acute $PI(4,5)P_2$ decrease ($p < 0.01$). Individual granules were more dynamic than control cells under the TIRF field (Figure 2J); particle-tracking assay revealed a slightly faster speed and shorter dwelling time. Different from those with chronic $PH_{PLC\delta1}$ expression (Figure 1), these results indicate that the rapid $PI(4,5)P_2$ decrease induces a prominent defect downstream of vesicle docking.

Impaired Ca^{2+} Signaling and Filamentous Actin (F-actin) dynamics, but Not Syntaxin1a Clustering, following Acute $PI(4,5)P_2$ Reduction

Next, we examined whether the rapid $PI(4,5)P_2$ decrease perturbs vesicle priming, its downstream step at Ca^{2+} triggering, or both. It is reported that syntaxin clusters partially colocalize with $PI(4,5)P_2$-enriched domains (Aoyagi et al., 2005; Kabachinski et al., 2014) and participate in LDCV docking and subsequent secretion (Gandasi and Barg, 2014; Barg et al., 2010; although it may not be required at the initial vesicle attachment to the PM [Yang et al., 2012]). To explore the spatial connection between vesicle fusion sites and syntaxin1a clusters in INS-1 cells, we imaged NPY-pHluorin and EGFP-syntaxin1a during the 60 mM KCl stimulation (Figures 3A–3D). NPY-pHluorin is invisible before fusion but becomes several-fold brighter than a single syntaxin1a cluster upon vesicle fusion. This characteristic response marks granule fusion sites, regardless of the presence of EGFP-syntaxin1a signal in each exocytosis event. In diffraction-limited TIRF images (Figures 3A, 3B, and 3D), most fusion events occurred at a EGFP-syntaxin1a cluster (83% events from total 111 fusion events in 10 cells). A smaller fraction of fusion events (17%) occurred in a region lacking an

EGFP-syntaxin1a cluster signal (Figures 3C and 3D), where the presence of unlabeled endogenous syntaxin1a molecules cannot be ruled out. Because NPY-pHluorin is invisible before membrane fusion, these data cannot distinguish whether the syntaxin1a cluster pre-exists before vesicles approach the PM or newly formed during stable docking (Gandasi and Barg, 2014).

This result raises a possibility that $PI(4,5)P_2$ decrease likely impairs vesicle priming through syntaxin1a cluster alteration. We tested this by directly monitoring syntaxin1a clusters in live cells following acute $PI(4,5)P_2$ decreases. Unexpectedly, light-activated $PI(4,5)P_2$ reduction did not change the size, density (Figures 3E and 3F), and dynamics of syntaxin1a clusters in these cells (Movie S3). This lack of effect contrasts with the disappearance of sytaxin1a clusters in PC12 cells after long-term overexpression of membrane-targeted synaptojanin-1 (van den Bogaart et al., 2011), as well as the chronic perturbation by overexpression of $PH_{PLC\delta1}$ (Figure 1). These data suggested different effects on syntaxin1a clusters from chronic and rapid $PI(4,5)P_2$ perturbations. Thus, syntaxin1a cluster alteration may play an important role in secretory regulation in chronic $PI(4,5)P_2$ perturbations, but such a role appears limited in the rapid $PI(4,5)P_2$ signaling in live cells.

It is known that $PI(4,5)P_2$ stimulates F-actin polymerization (Yin and Janmey, 2003; Saarikangas et al., 2010) and the latter modulates membrane trafficking and hormone secretion (Fan et al., 2015; Lanzetti, 2007; Wen et al., 2011). Thus, rapid $PI(4,5)P_2$ reduction may regulate vesicle trafficking and secretion by F-actin modulation. To test this, we monitored F-actin changes using Tractin-EGFP (as an F-actin probe; Johnson and Schell, 2009) in INS-1 cells co-expressing the optogenetic pairs. The rapid, light-induced 5′Ptase recruitment to the PM led to a partial disassembly of F-actin and a decrease of F-actin fluorescence intensity (Figure S1A), consistent with the $PI(4,5)P_2$ function in promoting F-actin formation (Saarikangas et al., 2010). This effect is reversible (through $PI(4,5)P_2$ re-synthesis) and reproducible in the same cell after a ~20-min break of blue light illumination (Figure S1D). Moreover, F-actin network appeared more active and dynamic after the rapid $PI(4,5)P_2$ decrease (Figure S1C; Movie S4). These F-actin alterations may contribute to the impaired granule docking and secretion during the rapid, global $PI(4,5)P_2$ decrease.

$PI(4,5)P_2$ is well known to regulate voltage-gated Ca^{2+} channels (Wu et al., 2002; Suh et al., 2010), a major source of intracellular Ca^{2+} concentration ($[Ca^{2+}]_i$) increase that drives vesicle fusion with supra-linear kinetics (Lou et al., 2005; Voets, 2000). To image $[Ca^{2+}]_i$ beneath the PM, we utilized a Ca^{2+} fluorescence probe GCAMP6s (Chen et al., 2013) anchored on the inner leaflet of the PM via a CAAX sequence (Figure 3G). Spontaneous oscillations of $[Ca^{2+}]_i$ were vigorous in many INS-1 cells at rest, and 60 mM KCl stimulation evoked large $[Ca^{2+}]_i$ elevations (Figures 3G–3I). After blue light activation in the cells co-expressing the iLID pair, the evoked responses were significantly smaller than control cells (Figures 3G–3I; Movie S5), consistent with the results measured by a cytosolic Ca^{2+} probe and patch-clamp (Xie et al., 2016). In addition, this $[Ca^{2+}]_i$ inhibition is fully reversible (Figures S1E–S1G). These data indicate that the impaired $[Ca^{2+}]_i$ signal is a key factor that accounts for the secretion defect during acute, cell-wide $PI(4,5)P_2$ decrease in the PM.

Rapid Optogenetic Control of Subcellular PI(4,5)P_2 Levels Selectively at Vesicle Docking Sites

Physiologically relevant PI(4,5)P_2 signal is often fast and confined to subcellular regions in order to achieve signaling specificity and efficiency in vivo. Secretory cells may utilize such local PI(4,5)P_2-mediated modulation at vesicle docking and release sites to regulate secretion, without significantly changing other PI(4,5)P_2-mediated cellular functions. Direct imaging studies showed a heterogeneous PI(4,5)P_2 distribution in intact live cells (Ji and Lou, 2016; Ji et al., 2015), although its nanometer-scale patterns are diverse in fixed samples ranging from dense nano-domains (van den Bogaart et al., 2011), microdomains (Ji et al., 2015; Fujita et al., 2009), or even distribution (van Rheenen et al., 2005). About 20% of dense core vesicles reside in PI(4,5)P_2-enriched regions on the fixed cell PM (Aoyagi et al., 2005), and this number increases to 50% when probed with $PH_{PLC\delta4}$-GFP (Kabachinski et al., 2014). However, the specific effect of these local PI(4,5)P_2 changes on vesicle trafficking remains unclear in live cells.

To address this question, we utilized the light-inducible CRY2-CIBN pair (Kennedy et al., 2010; Idevall-Hagren et al., 2012) but targeted CIBN (the anchor part) onto vesicles (Figure 4A) rather than the PM. After validating the efficiency of CRY2-CIBN pair in INS-1 cells (Figure S2), we cloned a chimera in which CIBN was tagged to vesicle membrane protein VAMP2 N terminus, so that blue light could recruit mCherry-CRY2-5′$Ptase_{OCRL}$ onto vesicles rapidly. We used the CRY2-CIBN pair rather than the iLID pair in this experiment because the CRY2 oligomerization tendency after light activation (Kennedy et al., 2010) may also enhance 5′Ptase recruitment onto vesicles. Consequently, mCherry-CRY2-5′$Ptase_{OCRL}$ that were recruited to docked vesicles, which directly contact with the PM at docking sites, would decrease local PI(4,5)P_2 levels selectively at this PM region without broadly affecting global PI(4,5)P_2 levels (Figure 4A). In INS-1 cells expressing the plasmids mCherry-CRY2-5′$Ptase_{OCRL}$ and CIBN-iRFP-VAMP2, vesicles were labeled by VAMP2 (Figure 4B, left; pseudo-color for iRFP), but not 5′$Ptase_{OCRL}$ signal at rest, indicating the predominant cytosolic presence of 5′$Ptase_{OCRL}$. Upon blue light illumination, we observed the rapid accumulation of mCherry-CRY2-5′$Ptase_{OCRL}$ fluorescence on CIBN-VAMP2-positive vesicles (Figure 4B, right, yellow spots). The good colocalization between 5′$Ptase_{OCRL}$ and VAMP2 fluorescence suggested an efficient recruitment of 5′$Ptase_{OCRL}$ onto the vesicles.

Next, we directly examine the local changes of PI(4,5)P_2 at vesicle docking sites by expressing this optogenetic pair (mCherry-CRY2-5′$Ptase_{OCRL}$-T2A-CIBN-VAMP2) and iRFP-$PH_{PLC\delta1}$ in INS-1 cells. Counterintuitively, we observed no obviously visible iRFP-$PH_{PLC\delta1}$ decrease at the PM regions with VAMP2-positive vesicles under TIRFM, despite the presence of efficient 5′$Ptase_{OCRL}$ translocation upon blue light activation (Figures 4C and 4D) and clear iRFP-$PH_{PLC\delta1}$ decreases in global manipulation (Figure S2). Because the local depletion requires a direct contact of 5′$Ptase_{OCRL}$ (on vesicles) with the PM and some vesicles visible under TIRFM are not always stably attached or docked on the PM, we only focus on those bright vesicles with a stable position (within an 195 x 195 nm region) for >4 s after 5′$Ptase_{OCRL}$ recruitment. Quantitative analysis revealed a small but significant decrease (4.2% ± 0.8%; n = 12 vesicles; $p < 0.005$) of iRFP-$PH_{PLC\delta1}$ signal after light

illumination, and this signal recovered after the vesicle moved away from the small vesicle-PM contacting region (Figure 4E). The similar results were observed from other cells (n = 7 cells; Figure S3A). Our imaging simulation suggested that the real PI(4,5)P_2 decrease at docking sites was stronger than the fluorescence loss detected by TIRFM because of the light diffraction of remaining iRFP-$PH_{PLC\delta1}$ signal surrounding the docking sites (Figure S3). Further quantitative simulations predicted a more severe PI(4,5)P_2 decrease at the local PM (nearly full depletion) in this experiment than the global manipulation (~60%; Figures S3D–S3G).

The Local PI(4,5)P_2 Decrease Impairs Vesicle Docking, but Not $[Ca^{2+}]_i$ in Live Cells

Next, we aim to examine how the specific PI(4,5)P_2 decreases at vesicle docking sites affect vesicle trafficking and exocytosis in INS-1 cells. Surprisingly, we observed dramatic vesicle undocking after the mCherry-5′$Ptase_{OCRL}$ translocation onto vesicles (Figures 5A–5C), contrasting with the cell-wide manipulation experiments. Upon blue light activation, ~50% vesicles labeled by mCherry-5′$Ptase_{OCRL}$ departed from the PM and left the TIRF field (Figures 5A–5C; Movie S6); some vesicles appeared insensitive to the local PI(4,5)P_2 decrease and remained on the PM for exocytosis upon stimulation (see below), presumably reflecting different priming status among docked vesicles. To distinguish the potential contribution of light-inducible CRY2 oligomerization (Kennedy et al., 2010) to this result, we replaced 5′$Ptase_{OCRL}$ with its enzyme-dead mutation (D523G; as confirmed in Figure S2D) as a control optogenetic pair. We observed no vesicle undocking (Figure 5B; Movie S6) despite light-inducible mCherry-5′$Ptase_{OCRL(D523G)}$ translocation occurring efficiently. This suggested a specific role of 5′$Ptase_{OCRL}$. Indeed, we noticed marginal levels of vesicle clustering in some cells during light activation from both 5′$Ptase_{OCRL}$ and its D523G mutant experiments, consistent with the low levels of light-inducible CRY2 oligomerization (Kennedy et al., 2010). However, this oligomerization effect should not affect our conclusion because the D523G mutant experiment did not show docking defect. This was further supported by the alternative experiment (Figure S4) using the iLID pair that has no oligomerization tendency (Hallett et al., 2016), in which we observed a similar vesicle undocking effect (Figure S4). These data uncover a previously unknown function of PI(4,5)P_2 in vesicle availability and docking at the PM, which specifically occurs upon the rapid PI(4,5)P_2 metabolism at vesicle docking sites in living cells.

To examine the effect of the local PI(4,5)P_2 changes on vesicle secretion, we tagged pHluorin to VAMP2 luminal domain (Figure 5D, bottom) so that vesicle fusion can be detected by a transient pHluorin flashing spot. In control cells expressing mCherry-CRY2-5′$Ptase_{OCRL(D532G)}$-T2A-CIBN-VAMP2-pHluorin, 60 mM KCl stimulation induced vigorous vesicle fusion as indicated by the overall increase of VAMP2-pHluorin fluorescence intensity on the PM (Figure 5D, top). Abundant individual fusion events can be identified during the stimulation (Figure 5E, top; Movie S7), suggesting an intact VAMP2-pHluorin function in supporting vesicle fusion after light-induced 5′$Ptase_{OCRL(D532G)}$ translocation onto vesicles. In contrast, in cells expressing mCherry-CRY2-5′$Ptase_{OCRL}$-T2A-CIBN-VAMP2-pHluorin, we observed ~36% (n = 12 cells for both groups; $p < 0.05$) decrease in those bright fusion events compared to controls (Figures 5E and 5F). Simple

analysis of VAMP-pHluorin intensity on the PM also revealed a significant amplitude decrease (Figure S5), indicating impaired vesicle secretion.

Interestingly, unlike the cell-wide experiments (Figures 3G–3I), the intracellular Ca^{2+} signal monitored by GCaMP6s-caax fluorescence was comparable to control cells after the blue-light-induced $5'Ptase_{OCRL}$ translocation onto vesicles (Figures 5G–5I), both at the initial and later stages of light activation (Figure 5I). Similar results were observed when cells were stimulated at 20 s after light activation. These results indicate a negligible role from the $[Ca^{2+}]_i$ modulation under this condition, suggesting that only a limited portion of Ca^{2+} channels are colocalized with docked vesicles in INS-1 cells given the well-documented role of $PI(4,5)P_2$ in Ca^{2+} channel regulation (Suh et al., 2010; also see Figures 3G–3I). In addition, we examined the local actin dynamics during the local $PI(4,5)P_2$ interruption. We found no significant changes of actin filaments during blue light activation under the resolution of TIRFM. This contrasts with a significant change of F-actin observed under the cell-wide $PI(4,5)P_2$ decrease (Figures S1A–S1D). This experiment highlights a specific role of the local $PI(4,5)P_2$ decrease at vesicle docking sites as compared to the global $PI(4,5)P_2$ decrease.

Collectively, these local $PI(4,5)P_2$ perturbation experiments suggest that, under the context of physiological condition, spatially confined $PI(4,5)P_2$ changes on the PM appears to regulate vesicle secretion primarily through vesicle tethering and docking, and their contribution in modulating Ca^{2+} triggering or actin remodeling is limited.

DISCUSSION

We tackle the spatial-temporal regulation of $PI(4,5)P_2$ in the secretory pathway by TIRFM and optogenetic approaches. Direct comparisons among different spatial-temporal patterns of $PI(4,5)P_2$ perturbations revealed a mechanistically distinct role for $PI(4,5)P_2$ to regulate individual vesicle trafficking in insulin-secreting cells. Remarkably, the rapid and subcellular decreases of $PI(4,5)P_2$ levels result in pronounced vesicle undocking from the PM, a previously unappreciated function of $PI(4,5)P_2$ in vesicle secretory pathway.

This study characterized individual vesicle trafficking under the rapid, localized, and direct $PI(4,5)P_2$ manipulation in intact cells. We show that vesicle tethering/docking is a primary target for fast, subcellular $PI(4,5)P_2$ signal in the vesicle trafficking pathway of INS-1 cells. This is not trivial because $PI(4,5)P_2$ signaling in living cells is fast and highly compartmentalized (Trexler et al., 2016). Moreover, β cells release insulin in biphasic fashion (Fan et al., 2015; Seino et al., 2011); rapid vesicle availability, tethering, and docking at the PM may become a rate-limiting step during sustained insulin release. In contrast, long-term (in days or months) and cell-wide $PI(4,5)P_2$ changes may occur less frequently, e.g., under certain unusual scenarios, such as pathological conditions or cell damage. Thus, the tight spatial-temporal control of $PI(4,5)P_2$ signaling becomes critical to β cell physiology.

The vesicle undocking induced by the local $PI(4,5)P_2$ changes is striking. Such function has not been appreciated before despite its established role in vesicle priming (Hay and Martin,

1993; Gong et al., 2005), Ca^{2+} triggering (Xie et al., 2016), and fusion (Bai et al., 2004). Our direct vesicle imaging revealed significant vesicle departure from the PM in the local $PI(4,5)P_2$ decrease experiments, suggesting an important role of local $PI(4,5)P_2$ in the secretory pathway upstream of vesicle priming. The cell-wide perturbations may have limited impact to the local $PI(4,5)P_2$ levels under vesicle docking sites and thus showed minor undocking effects. $PI(4,5)P_2$ is likely to stabilize vesicle tethering to the PM by directly interacting with synaptotagmin-1 (Bai et al., 2004; Park et al., 2015; de Wit et al., 2009; Jahn and Fasshauer, 2012) and/or syntaxin1a (Aoyagi et al., 2005; Gandasi and Barg, 2014; Murray and Tamm, 2009) before a stable docking and priming. The syntaxin1a clustering and F-actin showed little alteration during such local $PI(4,5)P_2$ perturbations and thus appeared unlikely to play a major role. It is unclear whether vesicle priming proteins, such as calcium-dependent activator protein for secretion (CAPS) (Martin, 2015; Grishanin et al., 2004; Kabachinski et al., 2014) and Munc-13 (Brose and Rosenmund, 2002; Kabachinski et al., 2014; Shin et al., 2010) contribute to this process because they can directly interact with $PI(4,5)P_2$ at the PM. It will be interesting to address these questions in future work.

This work directly demonstrated distinct effects and mechanisms of $PI(4,5)P_2$ regulation under different spatial and temporal $PI(4,5)P_2$ signaling: long-term versus acute interruptions and cell-wide versus localized $PI(4,5)P_2$ metabolism. Syntaxin1a clusters dispersed after chronic perturbations (van den Bogaart et al., 2011; also see Figure 1I); however, the rapid $PI(4,5)P_2$ decrease has little effect on syntaxin clustering (within ~30 min) in live cells, indicating that syntaxin1a cluster alteration may play a less prominent role than previously thought in mediating the acute $PI(4,5)P_2$ regulation of exocytosis. The different temporal $PI(4,5)P_2$ perturbations may reconcile some discrepancy in literature. For example, acute PI(4,5)P2 reduction inhibits Ca^{2+} channels (Suh et al., 2010), but chronic PI(4,5)P2 reduction in PIPK1γ KO cells does not (Gong et al., 2005).

Our data showed a different role of spatial $PI(4,5)P_2$ signaling in secretion. Acute, cell-wide $PI(4,5)P_2$ reduction causes a large decrease of Ca^{2+} signal (Figures 3G–3I), consistent with a paper published (Xie et al., 2016) when this work was under review. In contrast, the rapid and localized decrease of $PI(4,5)P_2$ levels selectively at vesicle-PM contact sites shows no detectable effect on $[Ca^{2+}]_i$ responses, suggesting a limited contribution from the $PI(4,5)P_2$-mediated Ca^{2+} channel modulation in this case. This result reflects the number of affected Ca^{2+} channels is limited; it is possible that the number of Ca^{2+} channels colocalized with docked vesicles was too low to affect the total Ca^{2+} channel activity or vesicle-channel coupling may not be tight enough. In contrast, this rapid subcellular $PI(4,5)P_2$ decrease leads to strong vesicle undocking, highlighting that vesicle docking/tethering is an effective target of $PI(4,5)P_2$ alteration during secretion in living cells, where rapid and local $PI(4,5)P_2$ changes frequently occur in order to achieve efficient and specific signaling. This $PI(4,5)P_2$ function is consistent with a recent observation of localized $PI(4,5)P_2$ alteration at release sites (Trexler et al., 2016).

In summary, the role of $PI(4,5)P_2$ in the secretory pathway varies with temporal and spatial features of $PI(4,5)P_2$ signaling, the choice of targeting to vesicle recruitment, docking/tethering, priming, or Ca^{2+} influx relying on the time and space of $PI(4,5)P_2$ changes.

Optogenetics and direct vesicle imaging revealed that rapid, subcellular $PI(4,5)P_2$ reduction at vesicle docking sites effectively modulates vesicle tethering and docking to the PM. Because $PI(4,5)P_2$ signaling under many physiological conditions is spatially confined and short lived, it may target vesicle docking, in coordination with its downstream function in vesicle priming and fusion, as a general mechanism to regulate secretion in vivo.

EXPERIMENTAL PROCEDURES

INS-1 Cell Cultures, DNA Constructs, and Molecule Cloning

Insulin-secreting INS-1 832/13 cells (Hohmeier et al., 2000; passages 50–65; from Dr. Christopher B. Newgard at Duke University) were cultured as described previously (Ji et al., 2015). These cells were seeded on the round coverslips pre-coated with 15 μg/mL fibronectin (Millipore) and followed DNA transfection using Lipofectamine 3000 (Life Technologies). Experiments were performed between 48 and 60 hr after the transfection unless otherwise specified. DNA cloning and constructs are detailed in the Supplemental Information.

Live-Cell Spinning Disk Confocal and TIRF Imaging

We used a Nikon Ti-E Eclipse inverted-microscope-based imaging system under the control of NIS-Elements AR software as described previously (Ji et al., 2015; Ji and Lou, 2016). All experiments were performed at 35°C–37°C; imaging buffers and procedures are described in the Supplemental Information.

Exocytosis events (NPY-pHluorin and VAMP2-pHluorin) were continuously imaged under TIRFM at 5 Hz (200 ms exposure time) with 2 × 2 binning (equivalent pixel size of 130 nm). For imaging NPY-pHluorin and EGFP-syntaxin1a (Figures 3A–3D), NPY-pHluorin was nearly invisible before vesicle fusion but produced a large fluorescence increase upon fusion, which can be identified regardless of pre-existence of EGFP-synaxin1A. For LDCV dynamics assay, images of NPY-EGFP and NPY-DsRed were acquired under TIRFM at 1 Hz (500 ms exposure time; 1 × 1 binning).

To achieve light-inducible $PI(4,5)P_2$ decrease, cells were identified first by red or infra-red fluorescence protein co-transfected. The blue light (488 nm laser; 1 s; 5%–10% total power)-induced translocation of $5'Ptase_{OCRL}$ (tagged with tgRFPt or mCherry) was always verified. For simultaneously imaging of enzyme translocation and $PI(4,5)P_2$ changes, iRFP-$PH_{PLC\delta1}$ and $5'Ptase_{OCRL}$ were monitored sequentially at red and infra-red channels. In the experiment testing syntaxin1a cluster changes after $PI(4,5)P_2$ depletion, we noticed that some cells showed no obvious iRFP-syntaxin1a clusters before laser illumination and we chose the cells with normal syntaxin1a clusters to examine the acute effect of $PI(4,5)P_2$ reduction. iRFP-syntaxin1a clusters were imaged at a 30-s interval with 647 nm (exposure = 500 ms), and tgRFPt-Micro-$5'Ptase_{OCRL}$ was imaged with a 561-nm laser together with a 488-nm laser (500 ms exposure, no binning, to activate and maintain optogenetic recruitment) before each iRFP frame.

To image vesicle undocking in the cells expressing mCherry-CRY2-$5'Ptase_{OCRL}$-T2A-CIBN-VAMP2, we first took an image in mCherry channel before activating $5'Ptase_{OCRL}$

recruitment to vesicles induced by a blue light pulse (1 s; 5%–10% of the total power). After confirming the efficient 5′Ptase$_{OCRL}$ translocation, we imaged vesicle movement every 30 s under TIRF illumination using the mCherry recruited onto vesicles as a marker. Both 561 nm (for mCherry imaging) and 488 nm (for optogenetic recruitment) were activated, and emission was collected through a 600/75-nm filter. For secretion experiments in the cells expressing mCherry-CRY2-5′Ptase$_{OCRL}$T2A-CIBN-VAMP2-pHluorin, we started blue light activation and maintained it for 10 min (1 s light pulse; 20 s interval) so that undocking effect reaches a steady-state level. Then, we acquired continuous fast pHluorin TIRF images (5 Hz; 200 ms exposure) during 60 mM KCl perfusion for 7 min to detect all the fusion events. The 488-nm laser used for pHluorin excitation was sufficient to maintain optogenetic activation.

For intracellular Ca^{2+} imaging with GCaMP6s-CAAX, we first confirmed the blue-light-induced 5′Ptase$_{OCRL}$ (with tgRFPt/mCherry) translocation to the PM (or vesicles) in the red channel and then started GCaMP6s-CAAX images at 1 Hz (100-ms exposure time). After 30 s baseline acquisition, we switch perfusion buffer from nES to a high K^+ solution for another 3 min. Among all cells tested with global PI(4,5)P_2 depletion, we occasionally noticed a small number of cells (2 out 12) lacked calcium responses presumably due to cell damage, and they were excluded from statistics. In local depletion experiments, we started GCaMP6s-CAAX imaging 10 min after the initial blue-light-induced translocation of 5′Ptase$_{OCRL}$ to vesicles, a time when secretion tests were performed. We also test the GCaMP6s-CAAX imaging at an early time before vesicle undocking but after 5′Ptase$_{OCRL}$ translocation and found a similar result (Figure 5I). Imaging analysis is described in detail in the Supplemental Information.

Statistics

All data are presented as mean ± SEM; *n* represented the cell number unless otherwise specified. Multiple cells from at least three batches of cell cultures were performed for each experiment. Statistic comparisons were evaluated by two-tail Student's t test, and the significance level of difference is denoted with asterisks (*$p < 0.05$; **$p < 0.01$; ***$p < 0.005$). The normality and variance of data were tested before t test, and data variances were compared between the tested groups.

Supplementary Material

Refer to Web version on PubMed Central for supplementary material.

Acknowledgments

We thank the following people for materials: Dr. Christopher B. Newgard at Duke for sharing INS-1 cells; Dr. Tomas Balla (NIH) for DNA plasmids of PH domains mCherry-PH$_{PLC\delta1}$ and EGFP-PH$_{PLC\delta1}$; Dr. Olof Idevall-Hagren and Dr. Pietro De Camilli (Yale University) for NPY-EGFP, iRFP-PH$_{PLC\delta1}$, mCherry-CRY2-5′Ptase$_{OCRL}$, and CIBN-EGFPcaax; Dr. Ed Chapman for VAMP2-pHluorin and NPY-DsRed and for sharing Imaris software; Dr. Erik Dent for Tractin-EGFP; Dr. Meyer Jackson for EGFP-syntaxin1a; Dr. Tobias Meyer for GCaMP6s-CAAX; and Dr. Brain Kuhlman for iLID plasmids pLL7.0 (hITSN1(1159-1509)-tgRFPt-SSPB R73Q and pLL7.0:Venus-iLID-CAAX). This work is supported by the NIH grants 5R01DK093953 (to X.L.) and 1R21NS101584-01 (to X.L.), the grant AAB1425-135-A5362 (to X.L.) from the University of Wisconsin-Madison, and 14PRE20380168 (to C.J.) from the American Heart Associate (AHA). Chen Ji is partially supported by AHA predoctoral fellowship.

References

Aoyagi K, Sugaya T, Umeda M, Yamamoto S, Terakawa S, Takahashi M. The activation of exocytotic sites by the formation of phosphatidylinositol 4,5-bisphosphate microdomains at syntaxin clusters. J. Biol. Chem. 2005; 280:17346–17352. [PubMed: 15741173]

Axelrod D. Cell-substrate contacts illuminated by total internal reflection fluorescence. J. Cell Biol. 1981; 89:141–145. [PubMed: 7014571]

Bai J, Tucker WC, Chapman ER. PIP2 increases the speed of response of synaptotagmin and steers its membrane-penetration activity toward the plasma membrane. Nat. Struct. Mol. Biol. 2004; 11:36–44. [PubMed: 14718921]

Balla T. Phosphoinositides: tiny lipids with giant impact on cell regulation. Physiol. Rev. 2013; 93:1019–1137. [PubMed: 23899561]

Bar-On D, Wolter S, van de Linde S, Heilemann M, Nudelman G, Nachliel E, Gutman M, Sauer M, Ashery U. Super-resolution imaging reveals the internal architecture of nano-sized syntaxin clusters. J. Biol. Chem. 2012; 287:27158–27167. [PubMed: 22700970]

Barg S, Knowles MK, Chen X, Midorikawa M, Almers W. Syntaxin clusters assemble reversibly at sites of secretory granules in live cells. Proc. Natl. Acad. Sci. USA. 2010; 107:20804–20809. [PubMed: 21076041]

Brose N, Rosenmund C. Move over protein kinase C, you've got company: alternative cellular effectors of diacylglycerol and phorbol esters. J. Cell Sci. 2002; 115:4399–4411. [PubMed: 12414987]

Chen TW, Wardill TJ, Sun Y, Pulver SR, Renninger SL, Baohan A, Schreiter ER, Kerr RA, Orger MB, Jayaraman V, et al. Ultra-sensitive fluorescent proteins for imaging neuronal activity. Nature. 2013; 499:295–300. [PubMed: 23868258]

Cremona O, Di Paolo G, Wenk MR, Lüthi A, Kim WT, Takei K, Daniell L, Nemoto Y, Shears SB, Flavell RA, et al. Essential role of phosphoinositide metabolism in synaptic vesicle recycling. Cell. 1999; 99:179–188. [PubMed: 10535736]

De Camilli P, Emr SD, McPherson PS, Novick P. Phosphoinositides as regulators in membrane traffic. Science. 1996; 271:1533–1539. [PubMed: 8599109]

de Wit H, Walter AM, Milosevic I, Gulyás-Kovács A, Riedel D, Sørensen JB, Verhage M. Synaptotagmin-1 docks secretory vesicles to syntaxin-1/SNAP-25 acceptor complexes. Cell. 2009; 138:935–946. [PubMed: 19716167]

Di Paolo G, De Camilli P. Phosphoinositides in cell regulation and membrane dynamics. Nature. 2006; 443:651–657. [PubMed: 17035995]

Di Paolo G, Moskowitz HS, Gipson K, Wenk MR, Voronov S, Obayashi M, Flavell R, Fitzsimonds RM, Ryan TA, De Camilli P. Impaired PtdIns(4,5)P2 synthesis in nerve terminals produces defects in synaptic vesicle trafficking. Nature. 2004; 431:415–422. [PubMed: 15386003]

Duan L, Che D, Zhang K, Ong Q, Guo S, Cui B. Optogenetic control of molecular motors and organelle distributions in cells. Chem. Biol. 2015; 22:671–682. [PubMed: 25963241]

Fan F, Ji C, Wu Y, Ferguson SM, Tamarina N, Philipson LH, Lou X. Dynamin 2 regulates biphasic insulin secretion and plasma glucose homeostasis. J. Clin. Invest. 2015; 125:4026–4041. [PubMed: 26413867]

Fujita A, Cheng J, Tauchi-Sato K, Takenawa T, Fujimoto T. A distinct pool of phosphatidylinositol 4,5-bisphosphate in caveolae revealed by a nanoscale labeling technique. Proc. Natl. Acad. Sci. USA. 2009; 106:9256–9261. [PubMed: 19470488]

Gandasi NR, Barg S. Contact-induced clustering of syntaxin and munc18 docks secretory granules at the exocytosis site. Nat. Commun. 2014; 5:3914. [PubMed: 24835618]

Gong LW, Di Paolo G, Diaz E, Cestra G, Diaz ME, Lindau M, De Camilli P, Toomre D. Phosphatidylinositol phosphate kinase type I gamma regulates dynamics of large dense-core vesicle fusion. Proc. Natl. Acad. Sci. USA. 2005; 102:5204–5209. [PubMed: 15793002]

Grishanin RN, Kowalchyk JA, Klenchin VA, Ann K, Earles CA, Chapman ER, Gerona RR, Martin TF. CAPS acts at a prefusion step in dense-core vesicle exocytosis as a PIP2 binding protein. Neuron. 2004; 43:551–562. [PubMed: 15312653]

Guntas G, Hallett RA, Zimmerman SP, Williams T, Yumerefendi H, Bear JE, Kuhlman B. Engineering an improved light-induced dimer (iLID) for controlling the localization and activity of signaling proteins. Proc. Natl. Acad. Sci. USA. 2015; 112:112–117. [PubMed: 25535392]

Hallett RA, Zimmerman SP, Yumerefendi H, Bear JE, Kuhlman B. Correlating in vitro and in vivo activities of light-inducible dimers: a cellular optogenetics guide. ACS Synth. Biol. 2016; 5:53–64. [PubMed: 26474029]

Hammond GR, Balla T. Polyphosphoinositide binding domains: key to inositol lipid biology. Biochim. Biophys. Acta. 2015; 1851:746–758. [PubMed: 25732852]

Hammond GRV, Fischer MJ, Anderson KE, Holdich J, Koteci A, Balla T, Irvine RF. PI4P and PI(4,5)P2 are essential but independent lipid determinants of membrane identity. Science. 2012; 337:727–730. [PubMed: 22722250]

Hay JC, Martin TF. Phosphatidylinositol transfer protein required for ATP-dependent priming of Ca(2+)-activated secretion. Nature. 1993; 366:572–575. [PubMed: 8255295]

Hay JC, Fisette PL, Jenkins GH, Fukami K, Takenawa T, Anderson RA, Martin TF. ATP-dependent inositide phosphorylation required for Ca(2+)-activated secretion. Nature. 1995; 374:173–177. [PubMed: 7877690]

Heo WD, Inoue T, Park WS, Kim ML, Park BO, Wandless TJ, Meyer T. PI(3,4,5)P3 and PI(4,5)P2 lipids target proteins with polybasic clusters to the plasma membrane. Science. 2006; 314:1458–1461. [PubMed: 17095657]

Hohmeier HE, Mulder H, Chen G, Henkel-Rieger R, Prentki M, Newgard CB. Isolation of INS-1-derived cell lines with robust ATP-sensitive K+ channel-dependent and -independent glucose-stimulated insulin secretion. Diabetes. 2000; 49:424–430. [PubMed: 10868964]

Holz RW, Hlubek MD, Sorensen SD, Fisher SK, Balla T, Ozaki S, Prestwich GD, Stuenkel EL, Bittner MA. A pleckstrin homology domain specific for phosphatidylinositol 4, 5-bisphosphate (PtdIns-4,5-P2) and fused to green fluorescent protein identifies plasma membrane PtdIns-4,5-P2 as being important in exocytosis. J. Biol. Chem. 2000; 275:17878–17885. [PubMed: 10747966]

Honigmann A, van den Bogaart G, Iraheta E, Risselada HJ, Milovanovic D, Mueller V, Müllar S, Diederichsen U, Fasshauer D, Grubmüller H, et al. Phosphatidylinositol 4,5-bisphosphate clusters act as molecular beacons for vesicle recruitment. Nat. Struct. Mol. Biol. 2013; 20:679–686. [PubMed: 23665582]

Idevall-Hagren O, Dickson EJ, Hille B, Toomre DK, De Camilli P. Optogenetic control of phosphoinositide metabolism. Proc. Natl. Acad. Sci. USA. 2012; 109:E2316–E2323. [PubMed: 22847441]

Imig C, Min SW, Krinner S, Arancillo M, Rosenmund C, Südhof TC, Rhee J, Brose N, Cooper BH. The morphological and molecular nature of synaptic vesicle priming at presynaptic active zones. Neuron. 2014; 84:416–431. [PubMed: 25374362]

Jahn R, Fasshauer D. Molecular machines governing exocytosis of synaptic vesicles. Nature. 2012; 490:201–207. [PubMed: 23060190]

James DJ, Khodthong C, Kowalchyk JA, Martin TF. Phosphatidylinositol 4,5-bisphosphate regulates SNARE-dependent membrane fusion. J. Cell Biol. 2008; 182:355–366. [PubMed: 18644890]

Ji C, Lou X. Single-molecule super-resolution imaging of phosphatidylinositol 4,5-biphosphate in the plasma membrane with novel fluorescent probes. J. Vis. Exp. 2016; 2016:54466.

Ji C, Zhang Y, Xu P, Xu T, Lou X. Nanoscale landscape of phosphoinositides revealed by the specific pleckstrin homology (PH) domains using single-molecule superresolution imaging in the plasma membrane. J. Biol. Chem. 2015; 290:26978–26993. [PubMed: 26396197]

Johnson HW, Schell MJ. Neuronal IP3 3-kinase is an F-actin-bundling protein: role in dendritic targeting and regulation of spine morphology. Mol. Biol. Cell. 2009; 20:5166–5180. [PubMed: 19846664]

Kabachinski G, Yamaga M, Kielar-Grevstad DM, Bruinsma S, Martin TF. CAPS and Munc13 utilize distinct PIP2-linked mechanisms to promote vesicle exocytosis. Mol. Biol. Cell. 2014; 25:508–521. [PubMed: 24356451]

Kennedy MJ, Hughes RM, Peteya LA, Schwartz JW, Ehlers MD, Tucker CL. Rapid blue-light-mediated induction of protein interactions in living cells. Nat. Methods. 2010; 7:973–975. [PubMed: 21037589]

Lanzetti L. Actin in membrane trafficking. Curr. Opin. Cell Biol. 2007; 19:453–458. [PubMed: 17616384]

Lou X, Scheuss V, Schneggenburger R. Allosteric modulation of the presynaptic Ca2+ sensor for vesicle fusion. Nature. 2005; 435:497–501. [PubMed: 15917809]

Martin TF. PI(4,5)P(2) regulation of surface membrane traffic. Curr. Opin. Cell Biol. 2001; 13:493–499. [PubMed: 11454457]

Martin TF. PI(4,5)P_2-binding effector proteins for vesicle exocytosis. Biochim. Biophys. Acta. 2015; 1851:785–793. [PubMed: 25280637]

Milosevic I, Sørensen JB, Lang T, Krauss M, Nagy G, Haucke V, Jahn R, Neher E. Plasmalemmal phosphatidylinositol-4,5-bisphosphate level regulates the releasable vesicle pool size in chromaffin cells. J. Neurosci. 2005; 25:2557–2565. [PubMed: 15758165]

Murray DH, Tamm LK. Clustering of syntaxin-1A in model membranes is modulated by phosphatidylinositol 4,5-bisphosphate and cholesterol. Biochemistry. 2009; 48:4617–4625. [PubMed: 19364135]

Nakatsu F, Baskin JM, Chung J, Tanner LB, Shui G, Lee SY, Pirruccello M, Hao M, Ingolia NT, Wenk MR, De Camilli P. PtdIns4P synthesis by PI4KIIIα at the plasma membrane and its impact on plasma membrane identity. J. Cell Biol. 2012; 199:1003–1016. [PubMed: 23229899]

Neher E, Sakaba T. Multiple roles of calcium ions in the regulation of neurotransmitter release. Neuron. 2008; 59:861–872. [PubMed: 18817727]

Park Y, Seo JB, Fraind A, Pérez-Lara A, Yavuz H, Han K, Jung SR, Kattan I, Walla PJ, Choi M, et al. Synaptotagmin-1 binds to PIP(2)-containing membrane but not to SNAREs at physiological ionic strength. Nat. Struct. Mol. Biol. 2015; 22:815–823. [PubMed: 26389740]

Pathak GP, Vrana JD, Tucker CLCPCN. Optogenetic control of cell function using engineered photoreceptors. Biol. Cell. 2013; 105:59–72. [PubMed: 23157573]

Rettig J, Neher E. Emerging roles of presynaptic proteins in Ca++-triggered exocytosis. Science. 2002; 298:781–785. [PubMed: 12399579]

Rickman C, Medine CN, Dun AR, Moulton DJ, Mandula O, Halemani ND, Rizzoli SO, Chamberlain LH, Duncan RR. t-SNARE protein conformations patterned by the lipid microenvironment. J. Biol. Chem. 2010; 285:13535–13541. [PubMed: 20093362]

Saarikangas J, Zhao H, Lappalainen P. Regulation of the actin cytoskeleton-plasma membrane interplay by phosphoinositides. Physiol. Rev. 2010; 90:259–289. [PubMed: 20086078]

Seino S, Shibasaki T, Minami K. Dynamics of insulin secretion and the clinical implications for obesity and diabetes. J. Clin. Invest. 2011; 121:2118–2125. [PubMed: 21633180]

Shin OH, Lu J, Rhee JS, Tomchick DR, Pang ZP, Wojcik SM, Camacho-Perez M, Brose N, Machius M, Rizo J, et al. Munc13 C2B domain is an activity-dependent Ca2+ regulator of synaptic exocytosis. Nat. Struct. Mol. Biol. 2010; 17:280–288. [PubMed: 20154707]

Sieber JJ, Willig KI, Kutzner C, Gerding-Reimers C, Harke B, Donnert G, Rammner B, Eggeling C, Hell SW, Grubmüller H, Lang T. Anatomy and dynamics of a supramolecular membrane protein cluster. Science. 2007; 317:1072–1076. [PubMed: 17717182]

Südhof TC. Neurotransmitter release: the last millisecond in the life of a synaptic vesicle. Neuron. 2013; 80:675–690. [PubMed: 24183019]

Suh B-C, Inoue T, Meyer T, Hille B. Rapid chemically induced changes of PtdIns(4,5)P2 gate KCNQ ion channels. Science. 2006; 314:1454–1457. [PubMed: 16990515]

Suh B-C, Leal K, Hille B. Modulation of high-voltage activated Ca(2+) channels by membrane phosphatidylinositol 4,5-bisphosphate. Neuron. 2010; 67:224–238. [PubMed: 20670831]

Szentpetery Z, Várnai P, Balla T. Acute manipulation of Golgi phosphoinositides to assess their importance in cellular trafficking and signaling. Proc. Natl. Acad. Sci. USA. 2010; 107:8225–8230. [PubMed: 20404150]

Toettcher JE, Voigt CA, Weiner OD, Lim WACPCN. The promise of optogenetics in cell biology: interrogating molecular circuits in space and time. Nat. Methods. 2011; 8:35–38. [PubMed: 21191370]

Trexler AJ, Sochacki KA, Taraska JW. Imaging the recruitment and loss of proteins and lipids at single sites of calcium-triggered exocytosis. Mol. Biol. Cell. 2016; 27:2423–2434. [PubMed: 27307587]

van Bergeijk P, Adrian M, Hoogenraad CC, Kapitein LCCPCE. Optogenetic control of organelle transport and positioning. Nature. 2015; 518:111–114. [PubMed: 25561173]

van den Bogaart G, Meyenberg K, Risselada HJ, Amin H, Willig KI, Hubrich BE, Dier M, Hell SW, Grubmüller H, Diederichsen U, Jahn R. Membrane protein sequestering by ionic protein-lipid interactions. Nature. 2011; 479:552–555. [PubMed: 22020284]

van Rheenen J, Achame EM, Janssen H, Calafat J, Jalink K. PIP2 signaling in lipid domains: a critical re-evaluation. EMBOJ. 2005; 24:1664–1673.

Varnai P, Thyagarajan B, Rohacs T, Balla T. Rapidly inducible changes in phosphatidylinositol 4,5-bisphosphate levels influence multiple regulatory functions of the lipid in intact living cells. J. Cell Biol. 2006; 175:377–382. [PubMed: 17088424]

Voets T. Dissection of three Ca2+-dependent steps leading to secretion in chromaffin cells from mouse adrenal slices. Neuron. 2000; 28:537–545. [PubMed: 11144362]

Wen PJ, Osborne SL, Zanin M, Low PC, Wang H-TA, Schoenwaelder SM, Jackson SP, Wedlich-Söldner R, Vanhaesebroeck B, Keating DJ, Meunier FA. Phosphatidylinositol(4,5)bisphosphate coordinates actin-mediated mobilization and translocation of secretory vesicles to the plasma membrane of chromaffin cells. Nat. Commun. 2011; 2:491. [PubMed: 21971506]

Wenk MR, Pellegrini L, Klenchin VA, Di Paolo G, Chang S, Daniell L, Arioka M, Martin TF, De Camilli P. PIP kinase Igamma is the major PI(4,5)P(2) synthesizing enzyme at the synapse. Neuron. 2001; 32:79–88. [PubMed: 11604140]

Wu L, Bauer CS, Zhen XG, Xie C, Yang J. Dual regulation of voltage-gated calcium channels by PtdIns(4,5)P2. Nature. 2002; 419:947–952. [PubMed: 12410316]

Xie B, Nguyen PM, Guček A, Thonig A, Barg S, Idevall-Hagren O. Plasma membrane phosphatidylinositol 4,5-bisphosphate regulates Ca(2+)-influx and insulin secretion from pancreatic β cells. Cell Chem. Biol. 2016; 23:816–826. [PubMed: 27447049]

Yang L, Dun AR, Martin KJ, Qiu Z, Dunn A, Lord GJ, Lu W, Duncan RR, Rickman C. Secretory vesicles are preferentially targeted to areas of low molecular SNARE density. PLoS ONE. 2012; 7:e49514. [PubMed: 23166692]

Yazawa M, Sadaghiani AM, Hsueh B, Dolmetsch RE. Induction of protein-protein interactions in live cells using light. Nat. Biotechnol. 2009; 27:941–945. [PubMed: 19801976]

Yin HL, Janmey PA. Phosphoinositide regulation of the actin cytoskeleton. Annu. Rev. Physiol. 2003; 65:761–789. [PubMed: 12471164]

Zenisek D, Steyer JA, Almers W. Transport, capture and exocytosis of single synaptic vesicles at active zones. Nature. 2000; 406:849–854. [PubMed: 10972279]

Highlights

- Different PI(4,5)P_2 spatiotemporal signaling regulates vesicle trafficking distinctly
- Rapid, cell-wide PI(4,5)P_2 reduction impairs Ca^{2+} signaling, but not syntaxin1a clusters
- Optogenetics allows control of PI(4,5)P_2 levels selectively at vesicle docking sites
- The localized PI(4,5)P_2 reduction undocks vesicles from the plasma membrane

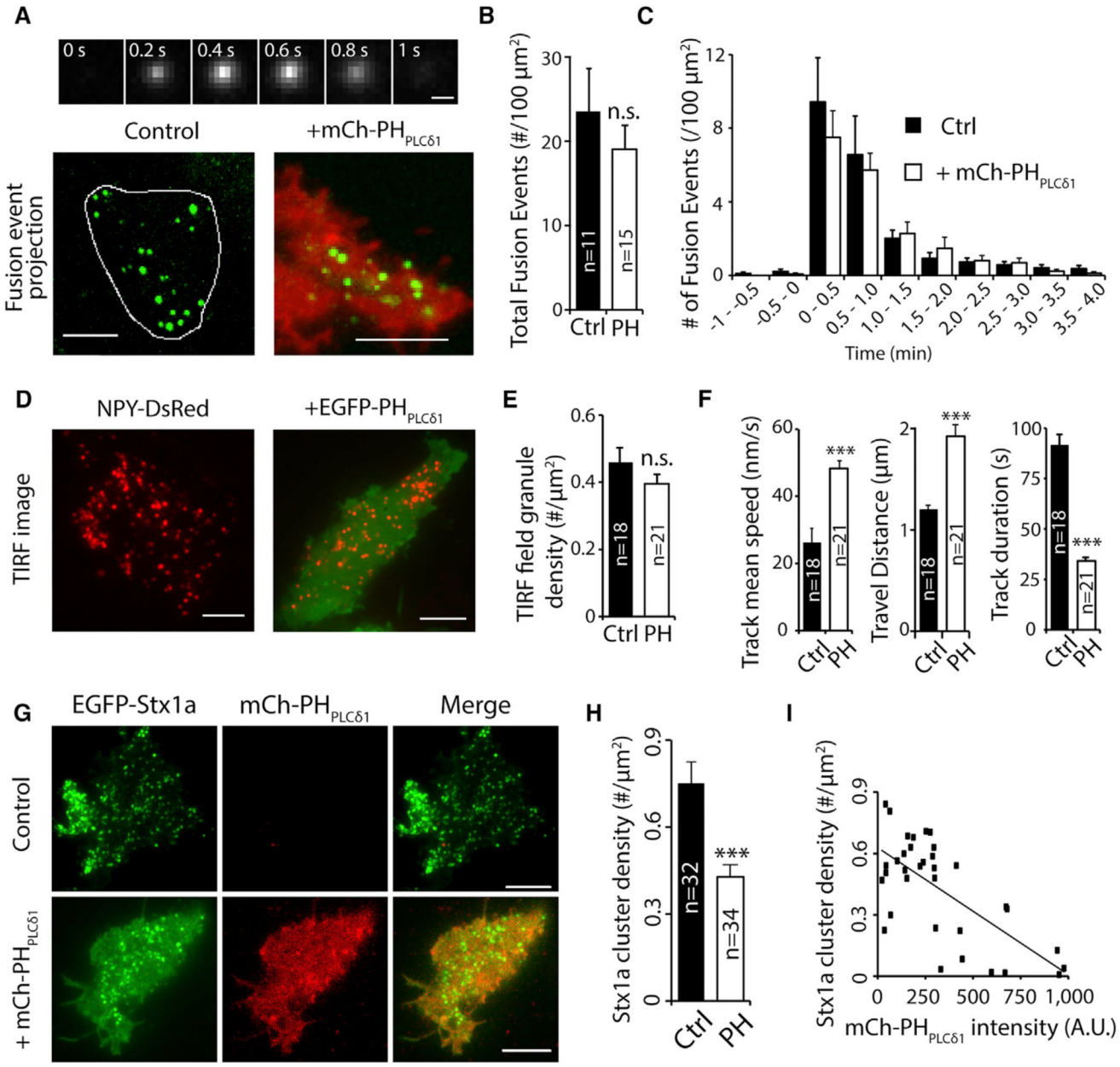

Figure 1. PI(4,5)P_2 Inhibition by PH_{PLCd1} Overexpression Impairs Granule Dynamics and Syntaxin1a Clustering

(A) A representative fusion event detected by NPY-pHluorin in an INS-1 cell (top); the bottom showed the time projection of fusion events during high K^+ stimulation (for 7 min) in a cell with (left) and without mCherry-$PH_{PLC\delta1}$ (right) expression. INS-1 cells were transfected with NPY-pHluorin alone (left) or with both NPY-pHluorin and mCh-$PH_{PLC\delta1}$ (right) for 48 hr and imaged under TIRFM. The green spots were fusion events, and the white line indicated the cell boundary.

(B and C) Total fusion events (B) and their time course (C) in the cells with (n = 11 cells) and without (n = 15 cells) co-expression of mCherry-$PH_{PLC\delta1}$ during 7 min high K^+ stimulation.

(D) LDCVs beneath the PM of INS-1 cells visualized by TIRFM. Cells were transfected with NPY-DsRed alone or together with EGFP-$PH_{PLC\delta1}$.
(E) Average LDCV density in the TIRF field in cells with or without EGFP-$PH_{PLC\delta1}$ co-expression.
(F) LDCV dynamics analysis from (D). Note the significant increase of granule mobility in cells overexpressing PH domain.
(G) TIRF images of EGFP-syntaxin1a (EGFP-Stx1a) clusters.
(H) The average density of EGFP-syntaxin1a clusters.
(I) EGFP-syntaxin1a cluster density negatively correlated with mCherry-$PH_{PLC\delta1}$ expression levels (n = 34 cells; $R^2 = 0.47$; Pearson correlation coefficient = −0.69).
The scale bars represent (D and G) 5 μm, (A) 500 nm (top), and 5 μm (bottom). The cell numbers tested in each experiment were indicated on the bar graphs (the same applies to other figures in this study). Error bars represent the SEM.

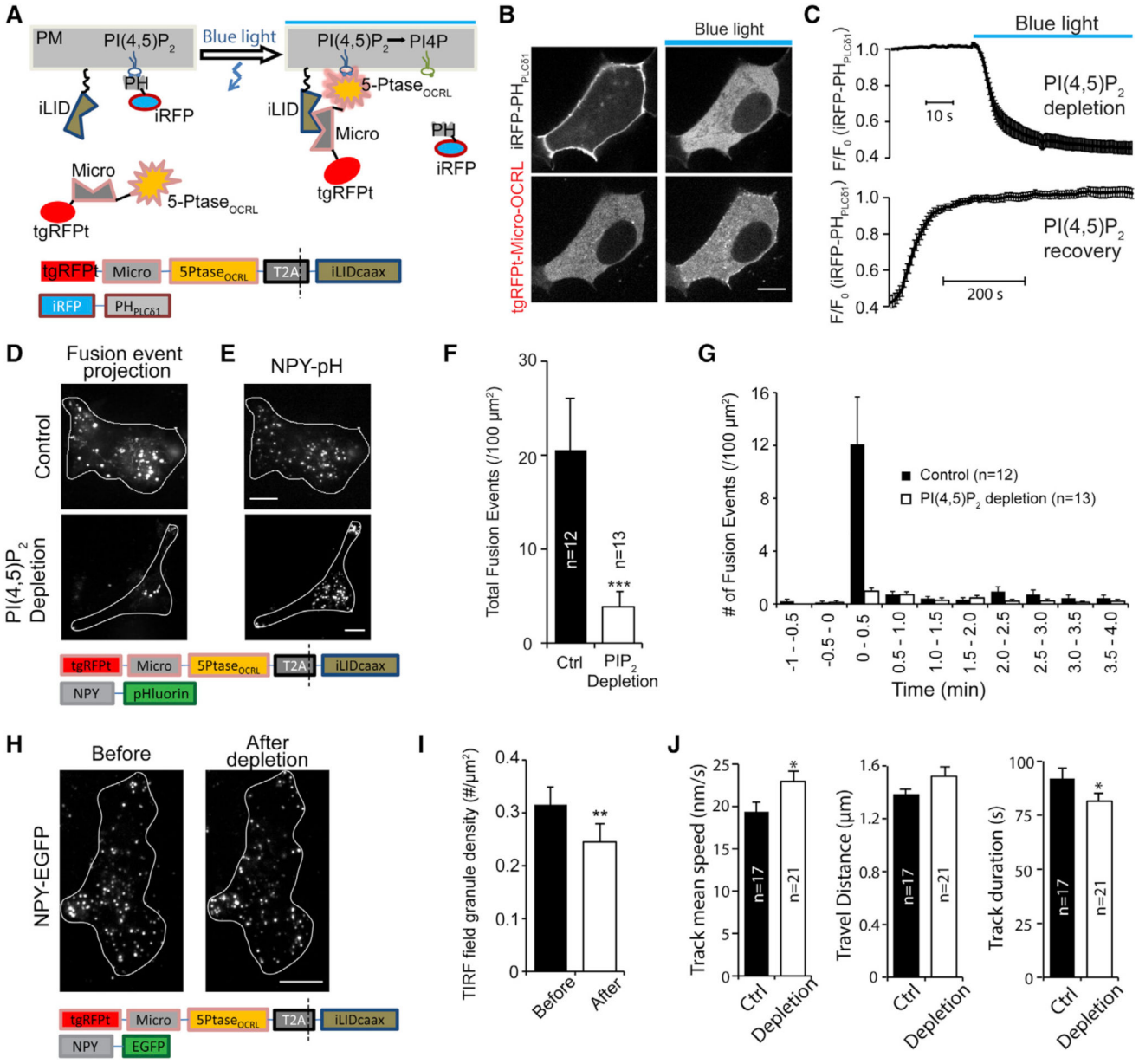

Figure 2. Rapid, Cell-wide PI(4,5)P_2 Decreases by Optogenetic Control Result in Distinct Defects in the Secretory Pathway

(A) The scheme of the optogenetic approach based on 5′-phosphatase (5′Ptase$_{OCRL}$) translocation to the PM to remove PI(4,5)P_2 by dephosphorylation. Bottom shows the construct scheme, where the dashed line indicates the T2A self-cleavage site after expression.

(B) Confocal images before and 30 s after the blue light activation (1 s; 10% of laser power) in an INS-1 cell expressing tgRFPt-Micro-5′Ptase$_{OCRL}$T2A-CIBNcaax and iRFP-PH$_{PLC\delta1}$.

(C) Average kinetics of blue-light-inducible PI(4,5)P_2 decrease and its recovery under live-cell TIRFM, as indicated by iRFP-PH$_{PLC\delta1}$ fluorescence intensity (n=13 cells).

(D) Total fusion events projection of NPY-pHluorin during 60 mM KCl stimulation from a control INS-1 cell (top) and a cell after the acute global PI(4,5)P_2 depletion (bottom). The

bottom scheme represents the constructs used in this experiment. Control cells (top) only expressed tgRFPt-Micro-5′Ptase$_{OCRL}$ and NPY-pHluorin. Images were acquired at 5 Hz (exposure time = 200 ms).

(E) TIRF images of granules (labeled by NPY-pHluorin) in the same cells shown in (D). Images were acquired with 405-nm laser excitation (525/50 emission filter) before depolarization.

(F and G) Total fusion events (F) and their time courses (G) after the acute global PI(4,5)P_2 depletion. Control cells expressed tgRFPt-Micro-5′Ptase$_{OCRL}$ and NPY-pHluorin, but not iLID. Cells were stimulated by 60 mM KCl for 7 min (***$p < 0.001$).

(H) TIRF images of NPY-EGFP granules before and after the acute global PI(4,5)P_2 depletion. Bottom shows the constructs used in (H)–(J).

(I) Granule density under TIRF field before and 10 min after a global PI(4,5)P_2 depletion (**$p < 0.01$; n = 22 cells).

(J) Granule dynamics in control cells (expressing tgRFPt-Micro-5′Ptase$_{OCRL}$ and NPY-EGFP) and cells after global PI(4,5)P_2 depletion (n = 17 cells in control; n = 21 cells under PI(4,5)P_2 decrease). The scale bar represents 5 μm.

Error bars represent the SEM.

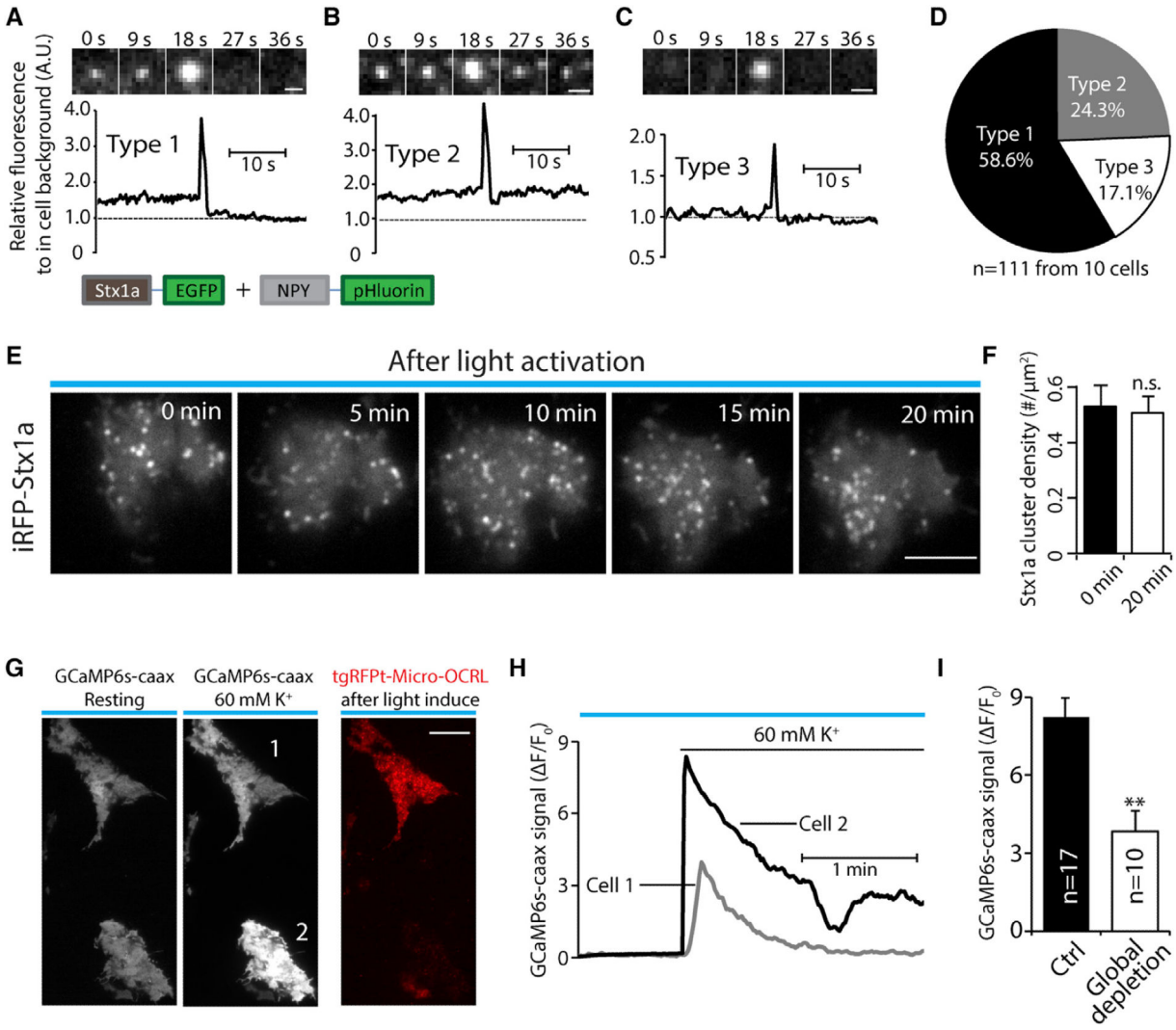

Figure 3. Impaired Intracellular Ca^{2+} Signaling, but Not Syntaxin1a Clustering, after Acute, Cell-wide $PI(4,5)P_2$ Decreases

(A–C) Three types of fusion events: with (A) or without (B) the dispersion of a syntaxin1a cluster after fusion and without a pre-existing syntaxin1a cluster (C).

(D) Summary of all fusion events (n = 111 events from 10 cells). Note the majority of LDCV fusion events occurred on or adjacent to a syntaxin1a cluster during 60 mM KCl depolarization. INS-1 cells were co-expressed with EGFP-syntaxin1a and NPY-pHluorin, and the latter was invisible before vesicle fusion. Fusion events were identified by a sudden, brighter NPY-pHluorin fluorescence increase upon vesicle fusion.

(E and F) Negligible impact of the acute global $PI(4,5)P_2$ depletion on iRFP-syntaxin1a cluster dynamics (E) and density (F). TIRF images of iRFP-syntaxin1a at different time after depletion were shown in (E), during which blue light was applied (1 s; 488-nm laser; 10% power) every 30 s to maintain $PI(4,5)P_2$ reduction.

(F) Average density before and 20 min after the global depletion of $PI(4,5)P_2$ is shown (n = 8 cells; p = 0.28).

(G) TIRF images of GCaMP6s-caax in the cells with and without global $PI(4,5)P_2$ depletion. Right panel showed the PM translocation of $5'Ptase_{OCRL}$ in cell 1, but not cell 2.
(H) The time courses of fluorescence changes.
(I) The average peak amplitude of GCAMP6s-caax responses in cells with (n = 10 cells) or without $PI(4,5)P_2$ global depletion (n = 17 cells) during 60 mM KCl perfusion (2.6 mM $CaCl_2$).
The scale bars represent 500 nm in (A)–(C), 5 μm in (E), and 10 μm in (G). Error bars represent the SEM.

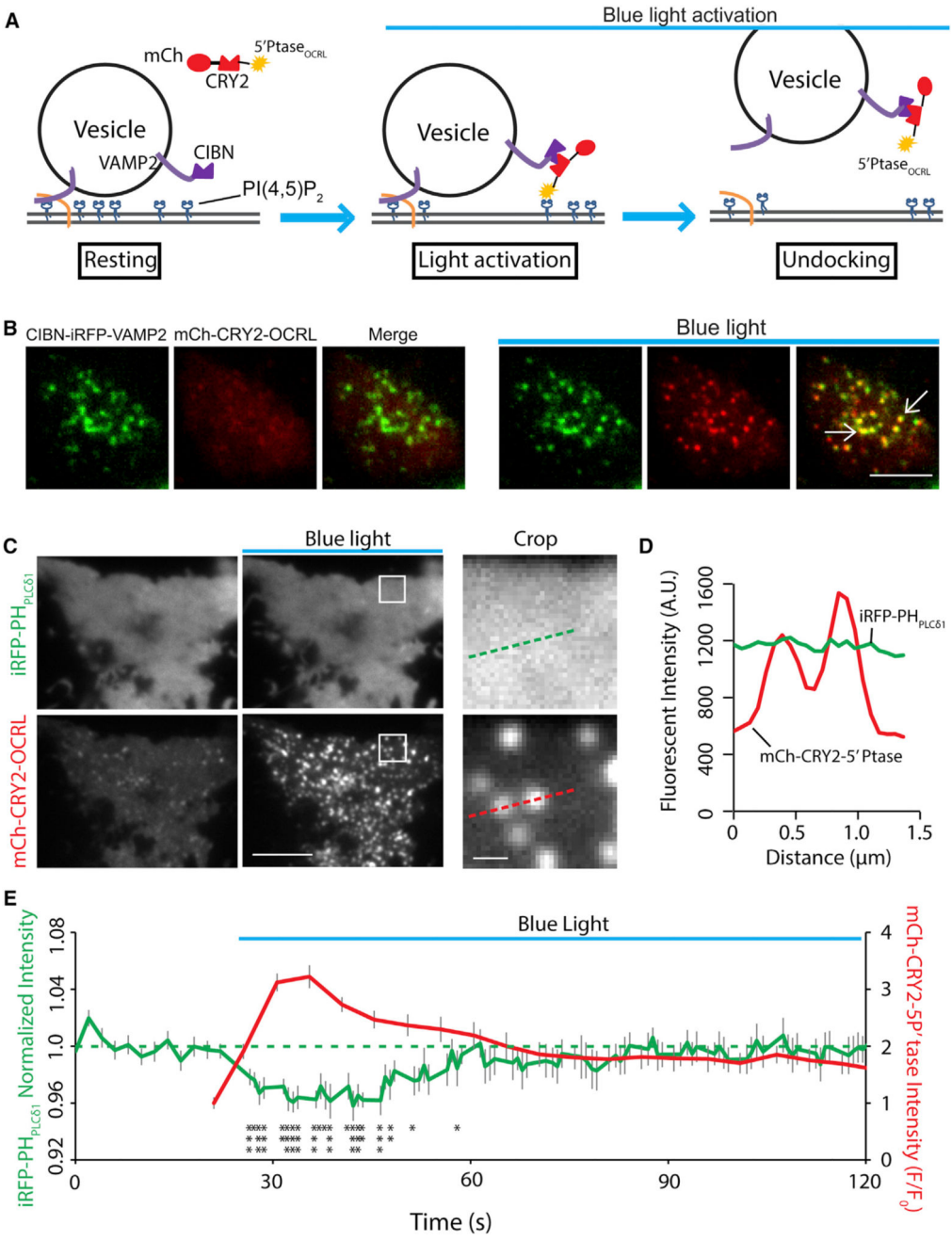

Figure 4. Rapid, Subcellular PI(4,5)P_2 Reduction Selectively at Vesicle Docking Sites Induced by Optogenetics

(A) The optogenetic strategy for rapid, localized PI(4,5)P_2 manipulation selectively at vesicle docking sites on the PM through light-inducible recruitment of 5′Ptase$_{OCRL}$ onto vesicle-PM contact regions.

(B) Blue light induced efficient recruitment of 5′Ptase$_{OCRL}$ onto vesicles in live INS-1 cells. VAMP2-labeled vesicles (in green, pseudo-color) and 5′Ptase$_{OCRL}$ (in red) were imaged by TIRFM before (left) and after (right) the blue light activation. Cells expressed both mCherry-CRY2-5′Ptase$_{OCRL}$ and CIBN-iRFP-VAMP2. Note the good colocalization

(arrows) between vesicles (CIBN-iRFP-VAMP2) and mCherry-CRY2-5′Ptase$_{OCRL}$ only after the blue light activation.

(C) TIRF images of iRFP-PH$_{PLC\delta1}$ and mCherry-CRY2-5′Ptase$_{OCRL}$ before and 10 s after the blue light activation (1 s; 10% power of the 488-nm laser). Right panel showed the enlarged views of boxed areas. Cells were transfected with mCherry-CRY2-5′Ptase$_{OCRL}$-T2A-CIBN-VAMP2 and iRFP-PH$_{PLC\delta1}$ for 48 hr before the experiment.

(D) The fluorescence intensity profiles of recruited phosphatase on vesicles and the corresponding iRFP-PH$_{PLC\delta1}$ along the lines in (C).

(E) Fluorescence intensity changes at vesicle docking sites before and after light-induced 5′Ptase$_{OCRL}$ recruitment onto vesicles. Both mCherry-CRY2-5′Ptase$_{OCRL}$ and iRFP-PH$_{PLC\delta1}$ were analyzed in the cell shown above, and the PM regions (195 × 195 nm square) with bright vesicles stabilized for at least 4 s were analyzed (n = 13 vesicles); those moving vesicles were excluded from analysis.

The scale bars represent 5 μm in (B) and (C) (left) and 500 nm in (C) (right).

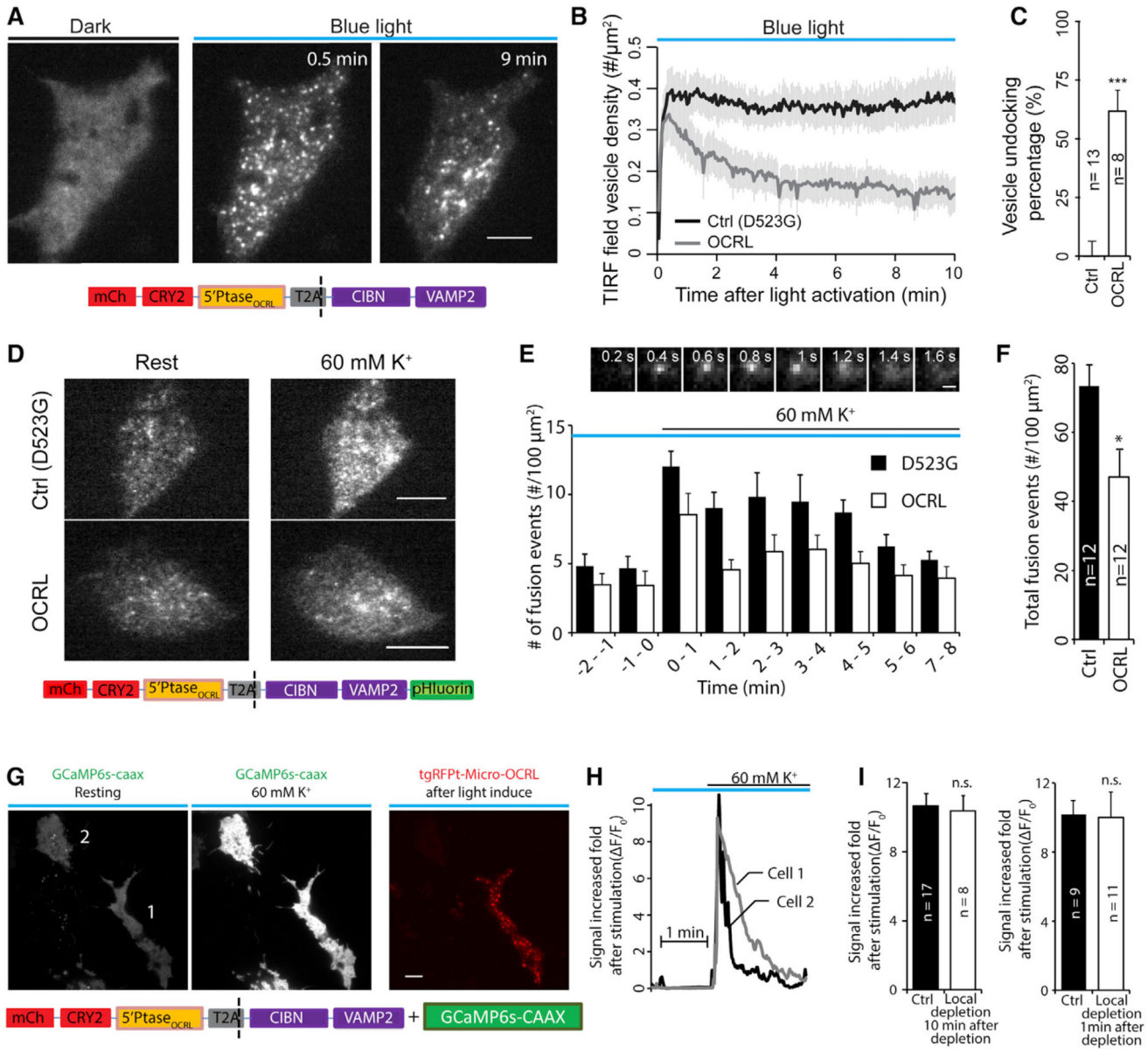

Figure 5. Rapid, Localized PI(4,5)P_2 Decreases at Vesicle Docking Sites Impair Vesicle Docking and Secretion, but Not Ca^{2+} Signal

(A) TIRF images of 5′Ptase$_{OCRL}$ before and 0.5 and 9 min after the blue-light-induced local PI(4,5)P_2 decrease. mCherry-CRY2-5′Ptase$_{OCRL}$ that was recruited on vesicles (middle panel) showed bright fluorescence and was used as a marker to monitor vesicle dynamics. Bottom showed the DNA construct (mCherry-CRY2-5′Ptase$_{OCRL}$-T2A-CIBN-VAMP2) scheme used.

(B) Vesicle density changes under TIRFM during continuous blue light activation. Cells with and without the local PI(4,5)P_2 reduction (n = 13 and 8 cells, respectively) were compared. Control cells expressing the D523G mutant of 5′Ptase$_{OCRL}$ (mCherry-CRY2-5′Ptase$_{OCRL}$(D523G)-T2A-CIBN-VAMP2) are shown.

(C) The relative changes of vesicle number after 10 min of blue light activation in control (OCRL (D523G) mutant; n = 8 cells) and treated cells (OCRL; n = 13 cells; $p < 0.001$).

(D) TIRF images of VAMP2-pHluorin before and after 60mM KCl stimulation in cells with and without local $PI(4,5)P_2$ decreases. Images were acquired at rest and 10 min after the blue-light-induced enzyme translocation. Control cells expressed the D523G mutant $5'Ptase_{OCRL}$ (mCherry-CRY2-$5'Ptase_{OCRL}$(D523G)-T2A-CIBN-VAMP2-pHluorin), which showed much strong pHluorin fluorescence increase after stimulation (top right). Bottom showed the construct scheme used for decreasing local $PI(4,5)P_2$ and detecting secretion.
(E) (Top) A typical fusion event detected by VAMP2-pHluorin in control INS-1 cells. (Bottom) Fusion event time course in the cells with (n = 12 cells) and without (n = 12 cells) the localized $PI(4,5)P_2$ decreases during 60 mM K^+ stimulation. Phosphatase translocation was pre-activated for 10 min before the high-speed VAMP2-pHluorin imaging (5 Hz; 200 ms exposures; 2 × 2 binning).
(F) Total fusion events (n = 12 cells for each group; $p < 0.05$).
(G) TIRF images of GCAMP6s-CAAX before and after 60 mM KCl stimulation in the cells with (cell 1) and without (cell 2) a local $PI(4,5)P_2$ decrease. Cell 1 co-expressed GCaMP6s-CAAX and mCherry-CRY2-$5'Ptase_{OCRL}$-T2A-CIBN-VAMP2, and cell 2 only expressed GCaMP6s-CAAX as a control. Bottom showed the constructs used in this experiment.
(H) GCAMP6s-CAAX fluorescent changes from the cells in (A).
(I) Average peak amplitudes of the evoked responses at 1 min or 10 min after the local $PI(4,5)P_2$ manipulation (in 2.6 mM extracellular Ca^{2+}).
The scale bars represent (A, D, and G) 5 μm and (E) 500 nm. Error bars represent the SEM.